

Copyright © 1973, by the author(s).
All rights reserved.

Permission to make digital or hard copies of all or part of this work for personal or classroom use is granted without fee provided that copies are not made or distributed for profit or commercial advantage and that copies bear this notice and the full citation on the first page. To copy otherwise, to republish, to post on servers or to redistribute to lists, requires prior specific permission.

PLASMA CONFINEMENT IN MULTIPLE-MIRROR SYSTEMS I: THEORY

by

A. Makhijani, A. J. Lichtenberg,
M. A. Lieberman, and B. G. Logan

Memorandum No. ERL-M388

1 March 1973

Electronics Research Laboratory
College of Engineering
University of California, Berkeley
94720

PLASMA CONFINEMENT IN MULTIPLE-MIRROR SYSTEMS I: THEORY

A. Makhijani, A. J. Lichtenberg,
M. A. Lieberman, and B. G. Logan

Department of Electrical Engineering
and Computer Sciences,
and Electronics Research Laboratory
University of California,
Berkeley, California 94720

ABSTRACT

For an intermediate mean free path regime where $\lambda \ll L$, the system length, but where $\lambda \gg \ell_m$, the scale length of the magnetic field variation, it is found that the confinement time τ_{mm} of ions in a multiple mirror system scales quadratically with the system length. When either inequality is not satisfied a transition is found to a scaling which is more closely proportional to L . For the high density regime this corresponds to MHD flow. By comparison with numerical and experimental results a criterion is found for the transition from the quadratic to the linear scaling. The value of $\tau_{mm} = ML^2/2\ell_c \bar{v}$ found from diffusion theory is in good agreement with a more accurate analytic treatment which is valid in the limit of $\lambda/M \ll \ell_c$, where M is the mirror ratio and ℓ_c is the cell length, and \bar{v} is the average ion velocity. Good agreement is also obtained with a self consistent numerical computation.

The work was supported in part by National Science Foundation Grant NSF-GK-27538 and by Air Force Office of Scientific Research Grant USAF-AFOSR-69-1754

* Present address is The Energy Policy Project, 1776 Mass Ave. N.W., Washington, D.C. 20036.

+ Present address is Naval Research Laboratory, Washington, D.C. 20375.

I. INTRODUCTION

During the last few years, interest has developed in multiple-mirror confinement systems as possible fusion reactors. Numerical calculations of particle containment in multiple-mirror systems have been performed using fixed scattering centers.^{1,2} With $\lambda\theta_c^2$, the mean free path mfp for scattering into a loss cone angle θ_c , comparable to the system length L , but much greater than the mirror spacing ℓ_c , Post found a containment time τ scaling roughly linearly with the number of mirror cells¹ (L increasing with the number of cells). With $\lambda\theta_c^2 \sim \ell_c \ll L$ however, Logan, et. al., found $\tau \sim L^2$, in agreement with diffusion theory.² Here λ is the Spitzer³ mfp for ion-ion collisions.

Taylor considered the effect of adding mirror cells of negligible length, with RF-assisted scattering, to the ends of a mirror device.⁴ Using particle conservation and with trapping probabilities per stopper near unity, he found a containment time for the center mirror cell increasing linearly with the number of stoppers (L constant). His analysis, applied to the case of stoppers of length equal to the center cell, predicts a quadratic increase of the total containment time with the number of stages, in agreement with the results of Logan et. al.²

From the kinetic theory, of ion and electron transport along a multiple mirror field, with $\ell_c \ll \lambda\theta_c^2 \ll L$, Budker et. al., find an

L^2 scaling for both heat and particle transport. In their analysis, electron effects were included using a self-consistent ambipolar electric field. They also found improved containment with sharp mirrors $[B/(dB/dz) \ll \ell_c]$ in contrast to a sinusoidal field variation. Preliminary experimental results have confirmed the $\tau \propto L^2$ scaling law and qualitatively given the predicted confinement time⁷.

In Section II of this paper, an approximate diffusion theory for particle and heat transport in a multiple-mirror system will be developed for a Maxwellian distribution, using a one-dimensional random walk description for each velocity group. The main purpose of this section is to develop formulas which span the range of parameters from $\lambda \theta_c^2 \ll \ell_c$ to $\lambda \theta_c^2 \gg \ell_c$ for comparison with experimental results.

In Section III, using a combination of kinetic theory and macroscopic conservation laws, the containment time is derived in the limit of collisional cells, $\lambda \theta_c^2 \ll \ell_c$ and collisionless mirrors $\lambda \theta_c^2 \gg B/(dB/dz)$. This limit, together with the results of Budker et. al.,^{4,5} bounds the values of containment time as found in Section II. It should be noted, however, that the entire range of m.f.p.'s from the limit given in Budker et. al. to the limit in Section III, are all part of the intermediate mfp regime in which $\tau \propto L^2$. For $\lambda \leq B/(dB/dz)$ the random walk approximation is no longer valid, leading to plasma flow conditions in which $\tau \propto L$. This regime, which we designate as the MHD flow regime, is analyzed in Section IV. Previous numerical computations, employing a fixed scattering center model for the collisions, cannot simulate the MHD regime. In order to explore, numerically, the transition between the intermediate m.f.p. regime and the MHD regime a numerical model has

been developed which includes drifts self-consistently. The results of this calculation are presented in Section V together with comparison of ion containment times obtained from diffusion theory and the macroscopic conservation laws. Results of experiments on plasma confinement in a multiple mirror device are presented in a companion paper,⁸ henceforth known as II, in which comparison of experiment with theory will be made.

II. DIFFUSION THEORY

Consider a symmetric multiple-mirror system as in Fig. 1, with S particles per unit area per unit time injected into the center in steady state. The mirror widths $\ell_m = B(dB/dz)^{-1}$ are assumed to be small compared to ℓ_c , so that the loss cone angle θ_c defined by

$$\sin^2 \theta_c = \frac{1}{M}, \quad (1)$$

where $M \equiv B_{\max}/B_{\min}$ is the mirror ratio, is a constant over the cell length ℓ_c . For many cells ($L \gg \ell_c$) large mirror ratios ($M \gg 1$), and sufficient source strength S such that the scattering mfp $\lambda \ll L$, particles will be trapped and untrapped many times before reaching the ends, so that their axial motion can be described by a random walk.

Since the distribution of velocities in such a system may approach a Maxwellian, the scattering distances for individual particles vary from distances much less than ℓ_c to distances much greater than ℓ_c . Considering the velocity groups which would have average step length ℓ_z much greater than ℓ_c (but ℓ_z still $\ll L$) the average step length ℓ_z and step time t can be estimated from average times t_1 and t_2 spent out and in the loss cone respectively. For particles at speed v , and $M \gg 1$ (small θ_c), we can estimate

$$t_2(v) \approx \tau_\theta(v) \theta_c^2 \approx \tau_\theta(v)/M, \quad (2)$$

where $\tau_\theta(v)$ is the scattering time at speed v for a mean-square deflection of $\bar{\theta}^2 = 1$ radian,² as calculated by Spitzer.⁶ We define the average step length between successive trappings, to be

$$\ell_z(v) \equiv \alpha t_z(v) v \quad (3)$$

where α is a proportionality constant to be determined by experiments.

Assuming the velocity-space density of ions at speed v in the loss cone is nearly the same as that out of the loss cone, (e.g. a Maxwellian) statistical mechanics gives the ratio of trapped time $t_1(v)$, to untrapped time $t_2(v)$, equal to the ratio of trapped to untrapped surface area at radius v in velocity space:

$$\frac{t_1(v)}{t_2(v)} = \frac{\cos \theta_c}{1 - \cos \theta_c} \approx 2M \quad (M \gg 1) \quad (4)$$

Equation (4) was found to qualitatively describe numerical results for t_1/t_2 .² For large M , $t_2(v)$ can be neglected compared to $t_1(v)$ in the total step time $t(v) = t_1(v) + t_2(v)$, Eq. (4) with Eq. (3) gives $t(v) \approx 2\tau_\theta(v)$. Note that for α of order unity and $\ell_z(v) \gg \ell_c$, t_1 is many bounce periods ℓ_c/v , so that the concept of trapping is well defined. We define a diffusion coefficient for the velocity group v satisfying $\ell_z(v) \gg \ell_c$ as

$$D(v) \equiv \frac{\ell_z^2(v)}{2t(v)} \approx \frac{\alpha^2 \tau_\theta(v) v^2}{4M^2} = \frac{\alpha \ell_z(v) v}{4M} \quad (5)$$

For velocity groups in which the scattering mfp.

$\lambda(v) \equiv t_z(v) \ll \ell_c$, the concept of trapping is not well defined, but the particles are nonetheless localized to each cell for many bounce periods with $M \gg 1$. For an isotropic distribution of ions per unit solid angle at speed v , the localization time (total step time) in a given cell is

$$t(v) = \frac{4\pi\ell_c}{2v \int_{\text{loss cone}} \cos \theta d\Omega} = 2M \frac{\ell_c}{v}, \quad (6)$$

where the integral is taken over one loss cone surface at radius v in velocity space. Note that $t(v)$ counts both the time spent by ions in the loss cone as well as out of the loss cone. When an ion crosses a mirror, it is considered to be localized to the center of the next cell, and the ion is counted as having taken a random walk step of length of length ℓ_c . The time to travel the distance ℓ_c is already counted in $t(v)$. For velocity groups with $\lambda(v) \ll \ell_c$, the diffusion coefficient is then

$$D(v) = \frac{\ell_c^2}{2t} = \frac{\ell_c v}{4M}. \quad (7)$$

To treat, approximately, the case of arbitrary ratios of $\lambda(v)/\ell_c$, we extend Eq. (5) and Eq. (7) beyond their valid limits, taking Eq. (5) for D for all ions with $\lambda(v)/M > \ell_c$ and Eq. (7) for D for all ions with $\lambda(v)/M < \ell_c$.

The average diffusion constant \bar{D} over a Maxwellian velocity distribution is

$$\bar{D} \equiv \frac{\int_0^{\infty} D(v) f_0 4\pi v^2 dv}{\int_0^{\infty} f_0 4\pi v^2 dv} \quad (8)$$

where $f_0 = \exp [-mv^2/2kT]$.

Using Eqs. (5) and (7) in the appropriate velocity regimes and evaluating the integrals, we obtain

$$\bar{D} = \left(\frac{\ell_c \bar{v}}{4M}\right) (G+H) \quad (9)$$

Here $\bar{v} = (8kT/\pi m)^{1/2}$, the average speed,

$$G(v_0) \equiv \left[1 - e^{-\frac{mv_0^2}{2kT}} \left(\frac{mv_0^2}{2kT} + 1\right)\right] \quad (10)$$

represents the contribution of "slow ions", $v < v_0$,

$$H(v_0) \equiv e^{-\frac{mv_0^2}{2kT}} \left[\frac{mv_0^2}{2kT} + 3 + 6\left(\frac{mv_0^2}{2kT}\right)^{-1} + 6\left(\frac{mv_0^2}{2kT}\right)^{-2} \right] \quad (11)$$

represents the contribution of "fast ions", $v > v_0$, and v_0 is obtained from $\lambda(v_0)/M = \ell_c$. The particle flux is then

$$F = -D\nabla n \quad (12)$$

The same model can be used to calculate the energy flux

$$Q = - \frac{\int_0^{\infty} \left(\frac{1}{2}mv^2\right) D(v) \nabla n f_0 4\pi v^2 dv}{\int_0^{\infty} f_0 4\pi v^2 dv} \quad (13)$$

Evaluating the integrals, we obtain

$$Q = -kT \left(\frac{\bar{v}}{4M} \right) (X + Y) \nabla n \quad , \quad (14)$$

where

$$X(v_0) \equiv \left[2G(v_0) - \left(\frac{mv_0^2}{2kT} \right)^2 e^{-\frac{mv_0^2}{2kT}} \right] \quad (15)$$

and

$$Y(v_0) \equiv \left[4H(v_0) + \left(\frac{mv_0^2}{2kT} \right)^2 e^{-\frac{mv_0^2}{2kT}} \right] \quad (16)$$

A convenient parameter to evaluate the functions G, H, X and Y is

$$\frac{\lambda^*}{\ell_c} \equiv \frac{\alpha \lambda(\bar{v}) \theta^2}{\ell_c} = \left(\frac{\bar{v}}{v_0} \right)^4 \quad (17)$$

where λ^* is the m f p for an ion of average speed to scatter into a loss cone angle. For $\lambda^*/\ell_c \ll 1$, the quantity $(mv_0^2/2kT)$ is large, the function G approaches unity, and the function H approaches zero. In this limit, \bar{D} has the minimum value D_{\min} given by Eq. (7) with $v = \bar{v}$. The ratio of \bar{D}_{\min}/\bar{D} , with \bar{D} given by Eq. (9), is plotted as a function of λ^*/ℓ_c in Fig. 2. For $\lambda^*/\ell_c \gtrsim .2$, the fast ion contribution to diffusion is greater than the slow ion contribution, and \bar{D} depends more on the mfp than on the cell length. For $\lambda^*/\ell_c \gg .2$, \bar{D} has the limiting form

$$\bar{D} = 3.7 \frac{\bar{\ell}_z(\bar{v})\bar{v}}{4M} = 3.7 \frac{(\alpha \lambda(\bar{v})\bar{v})}{4M^2} \quad (18)$$

The coefficient of 3.7 in Eq. (18) indicates that particles with velocities greater than the thermal velocity dominate the transport by diffusion, since they have much larger step lengths than $\lambda_z(\bar{v})$ when $\lambda_z(\bar{v}) \gg \lambda_c$. The factor 3.7 derived using our simple model agrees closely with the correction factor calculated by Hochstim and Masal⁹ for a diffusion coefficient varying as $T^{5/2}$.

The particle containment time τ for the case that $\lambda^*/\lambda_c \ll .2$ in all cells can be easily derived. Assuming T , \bar{v} , λ_c and the plasma cross sectional area to be the same in each cell, $\bar{D} = \bar{D}_{\min}$, given by Eq. (7) with $v = \bar{v}$. Particle conservation requires the particle flux F to be constant

$$-\bar{D}_{\min} \nabla n = \frac{S}{2} . \quad (19)$$

where S is the source strength. This indicates a linear density profile, $dn/dz = \text{const.} \equiv n_1/(L/2)$, with an average density $\bar{n} = \frac{1}{2} n_1$. For a discrete system of $K = L/2\lambda_c$ cells in a half length $L/2$; the maximum density n_1 in the center cell is given by

$$n_1 = K \Delta n , \quad (20)$$

where Δn is the density increment across each mirror. The containment time for this case is

$$T_{\text{mm}}(\text{max}) = \frac{\frac{1}{2} n_1 L}{2 \bar{D}_{\min} \nabla n} = \frac{L^2}{8 \bar{D}_{\min}} = \frac{ML^2}{2\lambda_c \bar{v}} \quad (21)$$

which is a maximum since the flux $2 \bar{D}_{\min} \nabla n$ is a minimum.

For $\lambda^*/\ell_c \gg 0,2$, for which \bar{D} is given by Eq. (18), \bar{D} is not constant with z since there is a density gradient with z and $\bar{D} \sim \lambda \sim \frac{1}{n}$. For systems with $\bar{D} \sim \frac{1}{n}$ in all cells, integration of $-\bar{D} \nabla n = \frac{S}{2}$ gives an exponential density profile:

$$\bar{D}(\bar{n}_{Ave}) n(z) = n_1 \exp\left[-\frac{Sz}{\bar{D}(\bar{n}_{Ave})\bar{n}_{Ave}}\right], \quad (22)$$

where $\bar{D}(\bar{n}_{Ave})$ is given by Eq. (18) evaluated at the average density \bar{n}_{Ave} . The containment time is

$$\tau_{min} = \frac{\bar{n} L}{S} = \frac{L^2}{\bar{D}(\bar{n}_{Ave})} [\ln(n_1/n(L))]^{-1}. \quad (23)$$

To determine the transport of energy Eq.(14) can be evaluated as a function of the parameter λ^*/ℓ_c . The resulting ratio Q/kTF is plotted in Fig. 2. The limits of $Q/kTF = 2, 4$ are in agreement with those calculated by Hochstim and Masal⁹ for the corresponding dependences of \bar{D} proportional to $T^{1/2}$ and $T^{5/2}$, respectively.

If we take the product $(Q/kTF)(\bar{D}_{min}/\bar{D})$ to obtain the relative variation of Q as a function of λ^*/ℓ_c we find that the product has a broad flat region near $\lambda^*/\ell_c = 1$, rising slowly for $\lambda^*/\ell_c < 0.2$ and falling slowly for $\lambda^*/\ell_c > 5$. Considering that the system length L and the density, and therefore λ^* , are held fixed, we obtain the result that the energy flux decreases slowly, i.e. the energy confinement time increases slowly with increasing number of mirrors. The limiting case is the corrugated magnetic field structure.^{5,6} For economy of design, long mirrors are desirable, and we therefore will concentrate our attention on the region for which $\lambda^*/\ell_c \approx 1$. In the following section, however, we consider the limit in which $\lambda^*/\ell_c \ll 1$, for which the containment time for a fixed system length L is maximized.

Up to this point nothing has been said about the effect of electrons on the ion containment time. Since $\lambda_e = \lambda_i$ for self scattering at $T_e = T_i$, consideration of electron motion alone leads to expressions for electron diffusion times similar to Eq. (21), except \bar{v}_e is used for \bar{v} . Thus electrons would initially diffuse m_i/m_e times faster than ions, resulting in an ambipolar electric field which regards the electrons. The ambipolar electric field increases the ion diffusion rate, with the well known result

$$D(\text{ambipolar}) = \bar{D}_i \left(1 + \frac{T_e}{T_i}\right) \quad (25)$$

for systems with no temperature gradients.

III. A THEORETICAL MODEL. Analytic Solution for $\lambda^*/M \ll \ell_c$

We consider the magnetic field geometry shown in Fig. 1, with $\lambda^*/M \ll \ell_c$. The magnetic field is constant in each cell, except in the mirror regions of length ℓ_m , where it is assumed that $r \ll \ell_m \ll \frac{\lambda^*}{M}$, with r the ion Larmor radius. The first inequality implies that the magnetic moment is conserved in the mirror region in the absence of collisions, and the second implies collisionless mirrors. The effects of the electron ambipolar potential are neglected and are corrected as in Eq. (25).

Since $\lambda^*/M \ll \ell_c$, the distribution function at the center of the i th cell is a drifting Maxwellian, characterized by the parameters n_i (density), v_{di} (drift velocity) and T_i (temperature). In the steady state, the particle and energy flow integrals are conserved (we ignore radial loss) and we have the following equations for cell i :

$$F \equiv v_z f_i d^3v \quad (26)$$

and

$$Q \equiv v_z^2 f_i d^3v, \quad (27)$$

where F and Q are constant in all cells with

$$f_i = \frac{n_i}{(2\pi)^{3/2} c_i^3} e^{-[v_x^2 + v_y^2 + (v_z - v_{di})^2]/2 c_i^2},$$

and $c_i^2 = \frac{kT_i}{m}$. We then have

$$F = n_i v_{di} \quad (28)$$

and

$$Q = n_i v_{di} (v_{di}^2 + 5 c_i^2) \quad (29)$$

From Eqs. (28) and (29), alone, we cannot determine the densities and temperatures in all cells, given $n_i v_{di}$ and T_i . The additional equation must come from the fact that the momentum flow in a given cell

$$P_i \equiv \int v_z f_i d^3v = n_i (v_{D_i}^2 + c_i^2), \quad (30)$$

for a drifting Maxwellian, is not conserved across a mirror. There is a net transfer of momentum to the magnetic field due to the unequal distribution functions on either side of the mirror and the specular reflection (in velocity space) of trapped particles by the mirror. Since the

mirrors are collisionless, all particles in the loss cone facing an adjacent cell are transmitted, as shown in Fig. 3, whereas all particles outside the loss cone are reflected. This causes the distribution function at the edge of the mirror to be symmetric in the trapped region of velocity space, but asymmetric in the loss cones. These considerations may be expressed by the following equations:

$$\begin{aligned}
 f_{i,r}(v,\mu) &= f_{i,r}(v_1, -\mu), & -\mu_c < \mu < \mu_c \\
 f_{i,r}(v,\mu) &= f_{i+1,l}(v,\mu), & -1 \leq \mu < -\mu_c \\
 f_{i,r}(v,\mu) &= f_{i+1,l}(v,\mu), & \mu_c < \mu \leq 1
 \end{aligned} \tag{31}$$

where $f_{i,l}(v,\mu)$ and $f_{i,r}(v,\mu)$ are the distribution functions at the left and right edges of cell i and μ_c is defined as $(1 - \frac{1}{M})^{1/2}$. To use Eq. (31) the form of the distribution functions $f_{i,l}$ and $f_{i,r}$ must be known. For infinite mirror ratios, there is no flow of particles through the mirrors and the steady state distribution function in each cell is a stationary Maxwellian. For large mirror ratios, we assume the form of the distribution function to be a stationary Maxwellian, with different density and temperature parameters in the loss cone and trapped regions (see Fig. 3).

We now consider a multiple mirror system with $(2N+1)$ cells and an external source of particles $S \text{ cm}^{-2} \text{ sec}^{-1}$ injected into the center cell. The injected particle velocities are assumed to be symmetric

in angle. The cells are numbered $-N, -N+1, \dots, -1, 0, 1, 2, \dots, N$. In the steady state the flow of particles in each axial direction is $F = S/2$. The integrals F, Q, P_i and P_{i+1} defined in Eqs. (26), (27) and (30) for a loss cone perturbed Maxwellian distribution with parameters n_a, T_a, n_b, T_b (see Fig. 3), for the mirror separating cells i and $i+1$, are given by

$$F = \frac{1}{(2\pi)^{1/2} M} (n_a c_a - n_b c_b) \quad (32)$$

$$P_i = \frac{n_a c_a^2}{2} (1 + \mu_c^3) + \frac{n_b c_b^2}{2} (1 - \mu_c^3) \quad (33)$$

$$P_{i+1} = \frac{n_a c_a^2}{2} (1 - \mu_c^3) + \frac{n_b c_b^2}{2} (1 + \mu_c^3) \quad (34)$$

$$Q = \frac{4}{(2\pi)^{1/2} M} (n_a c_a^3 - n_b c_b^3) \quad , \quad (35)$$

The boundary conditions at the mirror automatically insure particle flow and energy flow conservation across the mirror region. Eqs. (33) and (34) show that momentum is not conserved across a mirror for $\mu_c > 0$; i.e., for $M > 1$. Given n_i, v_{di} and T_i , we wish to find n_{i+1}, v_{di+1} and T_{i+1} , eliminating the intermediate unknowns n_a, T_a, n_b and T_b . However, we have only six equations for seven unknowns; one particle flow, one momentum flow and one energy flow conservation equation for each of the cells i and $i+1$. An approximate seventh equation is found in the limit of small drift. Equating energy flows in adjacent cells,

$$v_{di}^2 + 5 c_i^2 = v_{di+1}^2 + 5 c_{i+1}^2 \quad .$$

If the drift velocities are small compared to the thermal velocity, the above equation indicates that to a first approximation the system is isothermal. This is also borne out by the results of the numerical model (see Section V). We therefore make the assumption $T_a = T_b \equiv T$.

We solve for n_i , v_{di} and c_i by considering cell N at the right end of the system and iterate toward the center cell to obtain general expressions for the density, drift velocity and temperature in the i th cell, in terms of the parameters n_a , c_a at the right hand mirror of cell N . (If $i = N$ in Fig. 3, then $n_b \equiv 0$ at the right hand mirror).

We obtain:

$$n_i = \frac{5}{8} n_a \left[1 + \mu_c^3 \left(2(N-i) + 1 \right) \right] \quad (36)$$

$$v_{di} = \frac{4S}{5n_a} \left[\frac{1}{1 + \mu_c^3 \left(2(N-i) + 1 \right)} \right] \quad (37)$$

and
$$c_i = \frac{2c_a}{\sqrt{5}} \quad (38)$$

To express the parameters n_a and c_a in terms of the external source conditions, we define an average input particle velocity c_s such that $(\frac{1}{2} m c_s^2)S$ is the flow of energy into the system per unit area. Solving for n_a and c_a in terms of s and c_s , we finally obtain

$$n_i = \frac{5 \sqrt{2\pi} MS}{8 c_s} \left[1 + \mu_c^3 \left(2(N-i) + 1 \right) \right] \quad (39)$$

$$v_{di} = \frac{4}{5\sqrt{2\pi}} \frac{c_s}{M} \left[\frac{1}{1+\mu_c^3 (2(N-i)+1)} \right] \quad (40)$$

and

$$c_i = \frac{c_s}{\sqrt{5}} \quad (41)$$

The results (39) - (41) are insensitive to the assumed form of the distribution function near the mirrors, as can be shown by assuming another distribution function near the mirror to obtain results that differ by only small constant factors.¹³

We can now obtain the average containment time τ_c , for a $2N+1$ cell system, from the relation

$$\tau_c = \frac{\ell_c}{s} (n_0 + 2 \sum_{i=1}^N n_i) \quad (42)$$

Substituting Eq. (39) in Eq. (42) and performing the summation we have

$$\tau_c = \frac{5\sqrt{2\pi}}{8} \frac{M \ell_c}{c_s} (1 + 2N + 2\mu_c^3 N^2) \quad (43)$$

The assumptions of complete Maxwellianization in the cell midplanes and collisionless mirrors yields a value of τ_c from Eq. (43) that is an upper limit. Putting $N \approx \frac{L}{2\ell_c}$, $\mu_c \approx 1$, and using the definition of $c_s = (5\pi/8)^{1/2} \bar{v}$, Eq. (43) can be written as $\tau_c = (5/4)^{1/2} ML^2/2\ell_c \bar{v}$, which is seen to be $1.1 \tau_{mm}(\max)$ as given by Eq. (21), in good agreement with diffusion theory.

We contrast these analytic results with numerical values obtained in Section V. Taking $S = 5 \times 10^3$ particles $\text{cm}^{-2} \text{sec}^{-1}$, $M = 5$, and constant

velocity injection with $c_s = 7.8 \times 10^7$ cm/sec, we obtain $n_o \approx 4 \times 10^{17}$ particles cm^{-3} , $v_{do} \approx 6 \times 10^5$ cm/sec and $c_o = c_i = 3.44 \times 10^7$ cm/sec ($T_o = T_i = 2.5$ keV). When these parameters are used in the numerical model, the results are $n_o \sim 2 \times 10^{17}$ particles cm^{-3} , $v_{do} \sim 1.2 \times 10^6$ cm/sec, $T_o \sim 3$ keV and $T_4 \sim 2.6$ keV (see Figs. 8 and 9). The differences between the theoretical and numerical results may be attributed to the following factors related to the numerical parameters: (i) the mirror regions are not perfectly collisionless, (ii) the cells are not sufficiently long to isotropize the ions between mirrors.

IV. MAGNETOHYDRODYNAMIC THEORY

We consider the behavior of multiple mirror devices in the magnetohydrodynamic (MHD) limit. Taylor and Wesson¹⁰ have presented a solution for plasma flow in a converging nozzle. However, as we shall show below their solutions are not generally valid due to the assumption that sonic flow is always achieved at the throat. Here, we present the solution for both subsonic and sonic flow in the throat of a converging-diverging nozzle, and apply the results to the multiple mirror configuration.

The equations developed below result from combining the one dimensional equations for the steady-state flow of a neutral compressible gas¹¹ and the one dimensional MHD equations. Their validity is subject to the following restrictions: (i) isentropic potential flow, (ii) $\Delta B/B \ll \lambda/L$ where ΔB is the change in the magnetic field B over the Spitzer mean free path λ , and L is the characteristic length of the system, (iii) magnetic Reynolds number $\gg 1$, and (iv) infinite conductivity. Quantitative assessment of MHD validity to multiple mirrors is considered at the end of this Section.

With these restrictions, the mass continuity equation $\rho av = \text{const.}$ the adiabatic equation of state $p\rho^{-\gamma} = \text{const.}$, and the force equation

$$\frac{1}{2} \rho \nabla (v^2) - \rho \underline{v} \times (\nabla \times \underline{v}) = - \nabla p. + \frac{1}{\mu_0} (\nabla \times \underline{B}) \times \underline{B}$$

yield Bernoilli's equation for compressible gas flow

$$\frac{1}{2} v^2 + \omega = \text{const.} \quad (44)$$

Here ρ = mass density, v = fluid drift velocity, p = plasma pressure (assumed isotropic), a = plasma cross sectional area, \underline{B} is the magnetic field vector and ω = specific enthalpy ($d\omega = dp/\rho$). This description of MHD plasma flow is identical to compressible gas flow except that the plasma area $a(z)$ is an unknown function of the axial position z and must be determined from MHD considerations.

For an infinite conductivity plasma, the flux internal to the plasma ϕ_i and the flux external to the plasma ϕ_e are conserved; i.e.,

$$a(z)B_i(z) = \text{const.} \quad (45)$$

and

$$(A(z) - a(z))B_e(z) = \text{const.} \quad (46)$$

where $A(z)$ is the conducting wall area as shown in Fig. 4 . The plasma-vacuum interface boundary condition for streamline flow is

$$p + \frac{B_i^2}{2\mu_0} = \frac{B_e^2}{2\mu_0} \quad (47)$$

Solving Eqs. (44) - (47) for the plasma pressure $p(z)$ and plasma area $a(z)$ in terms of the initial conditions at the plasma inlet (see Fig. 4), denoted by subscript 1, we obtain

$$\left(\frac{p_1}{p_0}\right)^{1/\gamma} \left(\frac{v_1}{c_1}\right) \left(\frac{c_1}{c_0}\right) - \left(\frac{2}{\gamma-1}\right)^{1/2} \left(\frac{a}{a_1}\right) \left(\frac{p}{p_0}\right)^{1/\gamma} \left(1 - \left(\frac{p}{p_0}\right)^{\frac{\gamma-1}{\gamma}}\right)^{1/2} = 0 \quad (48)$$

and

$$\frac{p}{p_0} - \frac{1}{\beta_{i1}} \left(\frac{p_1}{p_0}\right) \left(\frac{a_1}{a}\right) \left\{ \alpha^2 \frac{\left(\frac{A_1}{a_1} - 1\right)^2}{\left(\frac{A}{a_1} - \frac{a_1}{a} - 1\right)^2} - 1 \right\} = 0 \quad (49)$$

where $\beta_{i1} \equiv \frac{p_0}{B_{i1}^2/2\mu_0}$ is the inlet internal plasma beta, and

$\alpha^2 \equiv B_{e1}^2/B_{i1}^2 = 1 + \beta_{i1}$, and the subscript 0 refers to plasma quantities corresponding to the zero drift velocity condition and has been used for convenience in normalization. We note that p_1/p_0 is specified in terms of the normalized initial flow velocity v_1/c_1 as

$$\frac{p_1}{p_0} = \left(\frac{\gamma-1}{2} \frac{v_1^2}{c_1^2} + 1 \right)^{-\frac{\gamma}{\gamma-1}} \quad (50)$$

For a given initial v_1/c_1 , β_{i1} and axial variation of the conducting wall area $A(z)/a_1$, Eq. (48) - (50) yield $p(z)/p_0$ and $a(z)a_1$. Some solutions are shown in Figs. 5 and 6. In Fig. 5 plots of $p(z)/p_0$ versus $A(z)/a_1$ are made for high and low β_{i1} for several values of initial velocity v_1/c_1 . We note from the form of the curves in Figs. 5 and 6 that for given values of v_1/c_1 and β_{i1} , it is impermissible to specify $A(z)/a_1$ less than some minimum value. This implies that there is a maximum wall ratio $R_w \equiv A_1/A_{\min}$ and a maximum plasma mirror ratio $R_p \equiv a_1/a_{\min}$. For given values of v_1/c_1 , β_{i1} and a_1 , it follows that there is a maximum flow W_{\max} where $W = \rho av$ which is given by¹¹

$$W_{\max} = \rho_* c_* a_{\min} = \gamma p_0 \rho_0 \frac{2}{\gamma+1} \frac{\gamma+1}{2\gamma-2} a_{\min} \quad (51)$$

where the subscript * denotes conditions at the plasma throat; i.e., at $a(z) = a_{\min}$. It is easily seen that for $v_1/c_1 < 1$ and $W < W_{\max}$, the flow velocity v is subsonic everywhere in the nozzle. Equation (51) shows that the maximum permissible flow W_{\max} is obtained for the case in which sonic velocity occurs at the throat. For $W = W_{\max}$, the flow in the diverging portion of the nozzle may be supersonic or subsonic, depending on the pressure conditions at the discharge portion of the nozzle (Fig. 4).

Solving for W using the conservation of mass, equation of state, and Bernailli's equation and using Eq. (51), W/W_{\max} is given by

$$W/W_{\max} = \frac{\gamma+1}{2} \frac{\frac{\gamma+1}{2\gamma-2} \left\{ \frac{v_1/c_1}{\left[\left(\frac{v_1}{c_1} \right)^2 \left(\frac{\gamma-1}{2} \right) + 1 \right]^{\frac{\gamma+1}{2\gamma-2}}} \right\} \frac{a_1}{a_{\min}}}{\left[\left(\frac{v_1}{c_1} \right)^2 \left(\frac{\gamma-1}{2} \right) + 1 \right]^{\frac{\gamma+1}{2\gamma-2}}} \quad (52)$$

It is clear that when $W = W_{\max}$, (52) explicitly determines v_1/c_1 ; i.e., v_1/c_1 is then not an independent initial condition.

We consider two types of initial conditions. If the nozzle is connected to a constant pressure reservoir ($p = p_0$, $v = 0$), then a solution similar to that of Taylor and Wesson is obtained; i.e., sonic flow in the throat. The minimum plasma area a_{\min} is obtained from Eqs. (48) - (52). W/W_{\max} is set equal to unity in the last equation. W_{\max} is then obtained from Eq. (51). Of greater interest to the problem of MHD flow in a steady state single or multiple mirror system is the case in which the flow W is a constant, determined by plasma injection conditions. For this case we calculate the variation of the plasma parameters as the wall mirror ratio R_w is varied (β_{11} is fixed). If $W < W_{\max}$ initially, W_{\max} decreases as R_w is increased, until the limit

$W = W_{\max}$ is reached and v_1/c_1 (and hence p_1/ρ_0) is determined by Eq. (52). If R_w is increased further and Q is maintained constant, the initial density ρ_1 must increase. A plot of ρ_1 versus R_w is shown in Fig. 7 for $\beta_{i1} = 0.1$.

To extend this analysis to multiple mirrors is simple for the case of interest where the cell mirror ratios increase in the direction of flow. If W_{mi} denotes the maximum permissible flow through the i^{th} mirror then we have $W_{mi} < W_{mj}$ for $i > j$. Therefore the flow in the system is subsonic throughout if it is subsonic at the inlet. The maximum flow is dictated by W_{mn} , where n is the index associated with the exit mirror. Since the flow is constant throughout the system, the confinement time of a test particle in the multiple mirror system with a fixed mirror ratio in the exit cell, is then proportional to the number of cells. This is in contrast with the intermediate density regime in which the confinement time scales as the square of the number of cells.

We now calculate the confinement time in a single cell in which the MHD assumptions are satisfied. Let S denote the flow of particles per unit plasma area per second, and n_1 the number density, both evaluated at the inlet. We specify S , a_1 , T_1 and β_{i1} , as the initial conditions. In the absence of any flow restrictions other than those represented by the mirror, $v_1/c_1 = \max$ in the throat. Therefore, from Eq. (52) we have (for $\gamma = 5/3$)

$$\frac{v_1}{c_1} = \frac{9}{16R_p} \left(\frac{1}{3} \left(\frac{v_1}{c_1} \right)^2 + 1 \right)^2$$

where $R_p \equiv a_1/a_{\min}$. For $R_p \geq 2$, $v_1/c_1 \approx 9/16 R_p$, giving for the single cell confinement time

$$\tau_c \leq \frac{\ell_c}{v_1} = \frac{16}{9} \frac{\ell_c R_p}{c_1}, \quad (53)$$

The inequality follows because the flow velocity is not a constant everywhere in the cell, but increases as B increases. Since v_1 is calculated at minimum B the actual confinement time is somewhat smaller than that given by Eq. (53), although for sharp mirrors with flat central regions the difference is not significant. For multiple mirrors we obtain an upper limit for the confinement time by replacing ℓ_c in the above Equations by the system half length $L/2$.

We now discuss the validity of MHD analyses following the work of Shkarofsky, Johnston and Bachynski.¹² We apply their analysis both to the conditions of our laboratory experiment, and to a conceptual fusion plasma configuration. For the MHD analysis we assumed scalar pressure and $\underline{E} + \underline{v} \times \underline{B} = 0$. From Ref. 12, the scalar pressure assumption is

valid if $\chi_1 \equiv \frac{m_i \ell_s v}{k T_i} \gg 1$ and $\chi_2 = \frac{\ell_s v}{v_o} \gg 1$, where ℓ_s is the scale

length over which the pressure changes v_o is the average drift velocity, m_i and T_i are the ion mass and temperature, and v is the ion-ion collision frequency.

For the lab plasma we choose parameters that correspond to the high density regime of the Berkeley multiple mirror experiments, with singly ionized potassium as the ion species. We take $T_i \approx 0.5\text{eV}$, $B = 2000$ Gauss, $n \approx 10^{11} \text{cm}^{-3}$, $\ell_c = 0.3\text{m}$, plasma radius = 1 cm and the injector source strength = 10^{16} particles $\text{cm}^{-2} \text{sec}^{-1}$. Since the plasma

is lost rapidly under these conditions, the characteristic drift velocity is $v_o \sim v_{th}/\bar{M}$, where \bar{M} is the mirror ratio averaged over the cell length. With $\bar{M} \approx 2$, $v_o \approx 10^5$ cm/sec, $\nu \approx 0.3 \times 10^4$ Hz and $\ell_s \approx \ell_c$, these parameters give $\chi_1 \approx 0.75$ and $\chi_2 \approx 1$, so that the assumption of scalar pressure is not completely satisfied. Furthermore, the $\tilde{J} \times \tilde{B}$ term and the resistivity term $\eta \tilde{J}$ in Ohm's law are not negligible. Despite this lack of clear applicability of MHD theory, a qualitative correspondence between the experimental results, and MHD theory exists. The periodic variations in density with magnetic field, found in the multiple mirror experiment, corresponds to that predicted by MHD theory and the confinement time increases linearly with the length of the system. However, if n is a factor of 5 smaller than the value used in the example (i.e. if $n \sim 2 \times 10^{10}$ cm), corresponding to a smaller collision frequency and $\chi_1 \approx \chi_2 \approx 0.2$, multiple mirror confinement effects can be observed in the system.⁷ (See also II). For the fusion plasma we select parameters roughly consistent with a fusion feasibility study presented in II. Deuterons are the ion species with $T_i \approx 5$ keV, $n_i \approx 10^{17}$ cm⁻³, $B = 100$ kG, and $\ell_c = 6.5$ m. We take $v_o \approx 2.5 \times 10^6$ cm/sec as calculated from the numerical model in the high density case with $S = 5 \times 10^{23}$ particles cm⁻² sec. (see Section V), $\nu \approx 2 \cdot 10^5$, and letting $\ell_s = \ell_c$ we obtain $\chi_1 = 0.14$ and $\chi_2 \gg 1$. Numerical studies in Section V, using the fusion parameters, above, indicate that multiple mirror effects are present at densities $n \lesssim 10^{17}$ cm⁻³, whereas for $n \gtrsim 2 \times 10^{17}$ cm⁻³, the variation of density from cell to cell is approximately that predicted by the MHD theory. This is clearly seen in Fig. 10 of Section V, where the density variation in a 10 cell system is plotted. In the four cells where

$n \sim 2 \times 10^{17} \text{ cm}^{-3}$, the density is almost constant from one cell to the next, but large differences in density exist for neighboring cells for $n \leq 10^{17} \text{ cm}^{-3}$.

In both the above examples, the scale length ℓ_s of the magnetic field variation has been taken equal to the cell length ℓ_c . This corresponds to a gradual field variation over the entire length of the cell. If the mirrors are peaked, then the scale length ℓ_s must be taken as the length of the mirror region (ℓ_m in Fig. 1). Using $\ell = \ell_m < \ell_c$ makes both χ_1 and χ_2 smaller and thus increases the range of densities over which multiple mirror effects can be obtained. We conclude that the transition from the intermediate mfp regime, in which the multiple mirror principle applies to the MHD flow regime, occurs for the parameters $\chi_1 = 0(1)$ and $\chi_2 = 0(1)$.

V. A NUMERICAL MODEL

In an earlier article² numerical calculations of containment time in a multiple mirror device were made using a fixed scattering center model for the collisions. Here we use a model in which the field particle densities, drift velocities and temperatures are included in a self consistent manner. The calculation procedure follows that of the earlier work.² A number of test particles are numerically followed through the multiple mirror system with the velocity vector of each test particle varied on each step. The variation is composed of two parts, an adiabatic change due to the variation of the magnetic field and a random change arising from small angle coulomb collisions with the background plasma. The random small angle scattering is computed in the center of mass frame of the background plasma which is drifting, and the velocity vector transformed

to the laboratory frame for computation of the adiabatic motion. The complete mathematical procedure is presented in Ref. 13. The confinement times of a large number of test particles are averaged to obtain a multiple mirror confinement time.

The values of the density, n_ℓ , drift velocity $v_{D\ell}$, and temperature T_ℓ of the field particles in cell number ℓ , that are used for the initial calculation of confinement time, are chosen either from the results of diffusion theory or from a fixed scattering center numerical model. From the average value of confinement time τ_ℓ in the ℓ^{th} cell the new values of the field parameters, to be used in the next iteration, are obtained from

$$n_\ell = \frac{S\tau}{\ell} ,$$

$$v_{D\ell} = \frac{S}{2n_\ell} , \quad (54)$$

$$kT_\ell = \frac{\pi}{8} m v_\ell'^2 ,$$

where v_ℓ' is the average test particle velocity in the drifting frame, and the source strength S is assumed constant throughout the calculation. The calculation procedure is then repeated until the results converge.

To obtain results appropriate to a fusion reactor design (see II), the mirror ratio was assumed to vary from cell to cell to hold the ratio λ^*/ℓ_c (see Eq. (17)) constant. To satisfy this condition with constant ℓ_c ,

$$\frac{M_\ell}{M_0} = \left(\frac{T_\ell}{T_0} \right)^2 \frac{n_c}{n_\ell} \quad (55)$$

where the subscript o refers to the quantities in the center cell. In order to allow for a variation of the sharpness of the mirror field the axial variation of the normalized magnetic field was chosen of the form

$$B(z) = \frac{1}{1+\gamma_\ell} [1 + \gamma_\ell \exp\{-\delta \sin^2(\frac{\pi z}{\ell_c})\}] \quad , \quad (56)$$

where $(1+\gamma_\ell) = M_\ell$ and δ , defining the sharpness of the axial field variation, was taken = 10 for the fusion plasma simulation. The source strength S was taken as 2.6×10^{23} particles $\text{cm}^{-2} \text{sec}^{-1}$ in order to obtain a center cell density $\sim 4 \times 10^{16} \text{m}^{-3}$ as is roughly appropriate for a reactor design as given in II. Test particles with an initial velocity of 7.8×10^7 cm/sec were injected at the minimum of the magnetic field, alternately into cell numbers 5 and 6 of a 10 cell system. The input field particle temperature was taken as constant (5 KeV) and the initial field particle densities and drift velocities were obtained from the results of the fixed scattering center model.² From Figs. 8 and 9 it is seen that an approximate convergence in density and temperature is obtained in 3 iterations.

To determine if the confinement time depends quadratically on the number of mirrors, numerical calculations for a 20 cell multiple mirror system were made using the same basic parameters as those used for the 10 cell system. In order to obtain a similar density regime as that used in the 10 cell case ($\approx 4 \times 10^{16}$ particles/ cm^3 in the center cells), the source strength was lowered to $S = 1.3 \times 10^{23}$ particles $\text{cm}^{-2} \text{sec}^{-1}$.

The results are shown in Table I.

TABLE I
Self-consistent numerical calculations
of multiple mirror confinement times.

# of cells	M_{\max}	M_{\min}	Optimized M?	Confinement time τ msec
10	7.2	4.0	Yes	0.866
20	7.2	4.0	No	2.6
20	16.8	4.0	Yes	3.1

In two runs with 20 cells the first used fixed mirror ratios, while the second, using a mirror ratio according to Eq. (55) increased the confinement time by about 20%. For both cases an approximately quadratic relation exists between the mirror ratio optimized 10 and 20 cell cases. The temperature extremes in the 20 cell cases were approximately the same as those obtained for the 10 cell case: T_{\min} (end cells) \approx 3.7 to 3.8 keV and $T_{\max} \approx$ 4.5 - 4.7 keV.

A comparison was also made between the computer run and some results obtained in the multiple mirror experiment.^{7,8} The experimental value for the axial confinement is \approx 17 msec⁷ and is in good agreement with a value of 15.4 msec which we obtain from the numerical calculation. Further details as well as other comparisons of theory and

experiment are given in II.

Since the confinement time in a multiple mirror system is sensitive to the ratio of ion-ion mean free path to cell length, runs were made with the numerical model using different source strengths. All other parameters were kept constant ($l_c = 6.5$ meters, input particle velocity = 7.8×10^7 cm/sec, particle species (deuterium), mirror ratio = 5 for each cell, number of cells = 10). The confinement time results are shown in Table II. (λ is the mean free path in the center cell.) We note from Table II that the confinement time first decreases and then increases with source strength. The high confinement time in the lowest source strength case is due to the fact that the system is essentially collisionless and that particles are injected into the system at an angle of 90° to the axis. As the source strength (density) is increased

TABLE II
Confinement time as a function
of source strength.

Particles $\text{cm}^{-2}\text{sec}^{-1}$	Confinement time τ_c msec	$\frac{n_{\text{max}}}{n_{\text{min}}}$	$\frac{\lambda}{(L/2)}$
1×10^{22}	≈ 0.47	≈ 3.2	6.3
5×10^{22}	0.32	3	1.95
1×10^{23}	0.53	4.9	0.46
5×10^{23}	1.48	3.8	0.046

the collision frequency increases and the confinement time decreases. In the intermediate mean free path regime, the confinement time again increases with increasing density. In the last case in Table II we are in a transition regime to short mean free path in the center cells with the intermediate mfp regime existing in the outer cells. In contrast, in the lower injection rate case of $S = 10^{23}$ particles $\text{cm}^{-2} \text{sec}^{-1}$ the densities in the end cells are too low for good confinement. For the higher density, the confinement times lie between the lower limit predicted by the MHD analysis in Section IV and the collisionless mirror region analysis of Section III. This behavior is illustrated by the density profile for the high density case in Fig. 10, showing the flattered MHD-type distribution in the center cells

In order to be useful a multiple mirror equilibrium must be stable against perturbations. The numerical iteration procedure may also be unstable, independently of the stability of the physical plasma. For example, in the low source strength case ($S = 10^{22}$ particles $\text{cm}^{-2} \text{sec}^{-1}$) five iterations were performed and numerical convergence was not obtained. (The confinement time shown in Table II is an average over the numerical oscillation). We present in Appendix A criteria for numerical and long-time physical stability. The analysis shows that convergence of the numerical procedure insures physical long-time stability, but not vice-versa. Experimentally^{7,8} it was found that stable multiple mirror density distributions could be found in the intermediate mfp regime.

VI. CONCLUSIONS

In conclusion, we have demonstrated that, under suitable conditions, a quadratic dependence of confinement time τ on the system length L can

be realized in a multiple mirror system. This result is obtained using an approximate diffusion analysis which is valid over a wide range of mean free paths for scattering out of a mirror loss cone λ/M , from $\lambda/M \ll \ell_c$ to $\lambda/M \gg \ell_c$ where λ is the ion-ion collision mfp, M is the mirror ratio, and ℓ_c is the length of a single mirror. The above result holds provided L is long compared to λ , and the mirror ratio M is sufficiently large. For high densities and small mirror ratios there is a transition to MHD flow in which τ is proportional to L . By comparison with numerical and experimental results a criterion is found for the transition from the intermediate mean free path regime, where multiple mirroring action can be found, to the MHD regime.

The value of τ , calculated from diffusion theory, is checked by a more accurate analytic treatment which is valid in the limit of $\lambda/M \ll \ell_c$, but with collisionless mirrors. It is found that the two theories give essentially the same value $\tau_{mm} = \frac{ML^2}{2\ell_c \bar{v}}$ where \bar{v} is the average speed.

A self consistent numerical analysis also gives a value of τ_{mm} in good agreement with that obtained from diffusion theory.

In a previous paper⁷ preliminary experimental results were reported which are in good agreement with the theoretical work presented here. In a companion paper⁸ the experimental results are considered in greater detail, and compared with the theory.

In this paper and in the companion paper we consider only axial confinement. Using the confinement times obtained in these two papers, a feasibility analysis of a fusion reactor, presented in II, indicates that the multiple mirror system is a possible alternative to other confinement systems. However, the system is at best average minimum B ,

and therefore subject to localized modes, in common with toroidal devices. Because the loss cone is nearly full, on the other hand, it should not be subject to velocity space instabilities. A theoretical and experimental investigation of the stability properties of multiple mirror devices is required.

APPENDIX A. NUMERICAL AND PHYSICAL STABILITY

Let

$$\tau_{i+1} = f(n_i)$$

and

$$n_{i+1} = \frac{S}{\ell_c} \tau_{i+1} = \frac{S}{\ell_c} f(n_i) ,$$

where the subscript i denotes the i^{th} iteration for the density and confinement time in cell ℓ , where, for convenience, the subscript ℓ has been omitted. Equilibrium between the test particles and field particles is obtained when $n_{i+1} = n_i = n_e$. To derive the condition for numerical convergence we expand τ_i , n_i and f about their equilibrium values. For the difference variables we then have

$$\Delta\tau_{i+1} = \frac{df}{dn} \Delta n_i \tag{A1}$$

$$\Delta n_{i+1} = \frac{S}{\ell_c} \Delta\tau_{i+1} \tag{A2}$$

From Eqs. (A1) and (A2) we have

$$\Delta n_{i+1} = \left(\frac{S}{\ell_c} \frac{df}{dn} \right)^i \Delta n_i \tag{A3}$$

Thus, for a fixed S , a stable numerical equilibrium is obtained if

$$\left| \frac{S}{\ell_c} \frac{df}{dn} \right| < 1 \quad (A4)$$

Inequality (A4) must be satisfied in each cell for the numerical procedure to converge. In the numerical procedure we make discrete jumps at each iteration between the curves $\tau_\ell = \frac{\ell_c n_\ell}{S}$ and $\tau_\ell = f(n_\ell)$, as shown in Fig. 11. We commence the procedure at some value of density n_a and the numerical procedure converges or does not converge according as inequality (A4) is or is not satisfied. The oscillation shown in Fig. 11b was observed for the first case in Table II. For the physical system, the situation is somewhat different. We create a perturbation in density so that the density is n_a instead of the equilibrium value n_e . If the slope $\frac{df}{dn}$ of the curve $\tau_\ell = f(n_\ell)$ is smaller than ℓ_c/S (the slope of the line $\tau_\ell = \frac{\ell_c n_\ell}{S}$) then a change in density from the equilibrium value will tend to restore the density and confinement time to the equilibrium values. The opposite will occur if $\frac{df}{dn} > \frac{\ell_c}{S}$ (see Fig. 11). This must hold since the curve $\tau_\ell = f(n_\ell)$ represents a physical property of the system and the confinement time and the density of the system must always lie on the curve.

Therefore whenever

$$\frac{df}{dn_\ell} < \frac{\ell_c}{S} \quad (A5)$$

holds for every cell in the system, the system will be stable to density perturbations on time scales long with respect to the confinement time. The last qualification is necessary since the entire

formulation is quasi steady state and is therefore not applicable to temporal fluctuations comparable to or smaller than the confinement time. We note that inequality (A4) implies (A5), but not vice versa. This means that a convergence of the numerical procedure implies long-time physical stability, but that the reverse is not necessarily true.

For the first case of Table II, a value of $\left| S \frac{df_{\ell}}{dn_{\ell}} \right| \sim 30$, and hence a numerical convergence was not obtained. For the 10 cell case with $S = 2.6 \times 10^{23} \text{ m}^{-2} \text{ sec}^{-1}$, $\left| \frac{S}{\ell_c} \frac{df_{\ell}}{dn_{\ell}} \right| \sim 0.3$ indicating the convergence that was found numerically.

REFERENCES

1. R. F. Post, Phys. Rev. Lett. 18 232 (1967)
2. B. G. Logan, A. J. Lichtenberg, M. A. Lieberman and A. Makhijani, Phys. Rev. Lett. 28 144 (1972)
3. L. Spitzer, Jr., Physics of Fully Ionized Gases, 2nd Ed. J. Wiley, 1962
4. J. B. Taylor, "Multiple Mirrors and R. F. Stoppers," in Culham Laboratory Report CLM-R94, p. 27, U.K.A.E.A., England (1969)
5. G. I. Budker, V. V. Mirnov and D.D. Ryutov, ZHETF Pis. Red. 14 320 (1971)
6. V. V. Mirnov and D. D. Ryutov, Nuclear Fusion 12 627 (1972)
7. B. G. Logan, I. G. Brown, M. A. Lieberman and A. J. Lichtenberg, Phys. Rev. Lett. 29 1439 (1972)
8. B. G. Logan, I. G. Brown, M. A. Lieberman and A. J. Lichtenberg, Phys. of Fluids (this issue)
9. A. R. Hochstim and G. A. Masal, Chap. IV in Kinetic Processes in Gases and Plasmas, Academic Press, 1969
10. J. B. Taylor and J. A. Wesson, Nuclear Fusion 5 159 (1965)
11. L. D. Landau and E. M. Lifshitz, Fluid Mechanics, Pergamon Press, New York, 1959
12. I. P. Shkarofsky, T. W. Johnston and M. P. Bachynski, The Particle Kinetics of Plasmas, Addison Wesley, Palo Alto, 1966
13. A. Makhijani, "Theoretical and Numerical Investigation of Steady State Multiple Mirror Plasmas", Ph.D. Thesis, Univ. of Calif. Berkeley, 1972

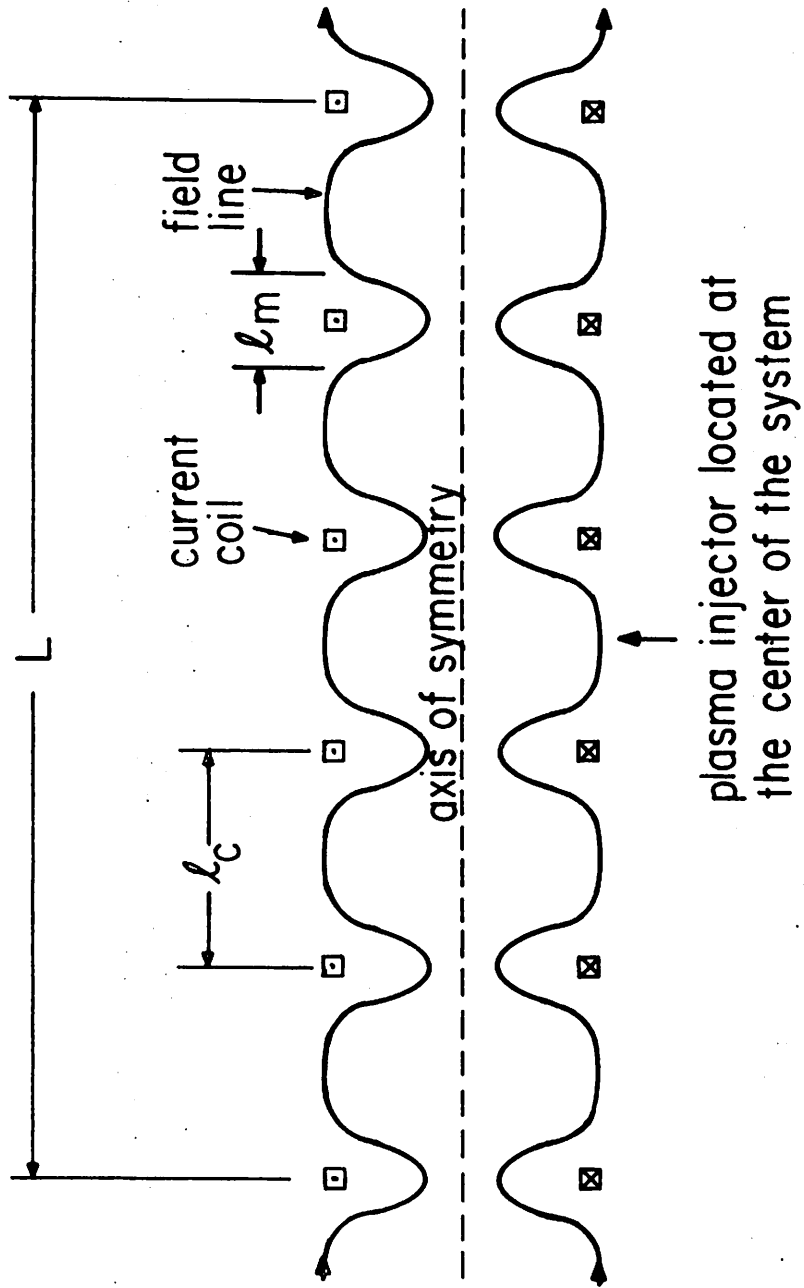


Fig. 1 Multiple Mirror Magnetic Field Geometry

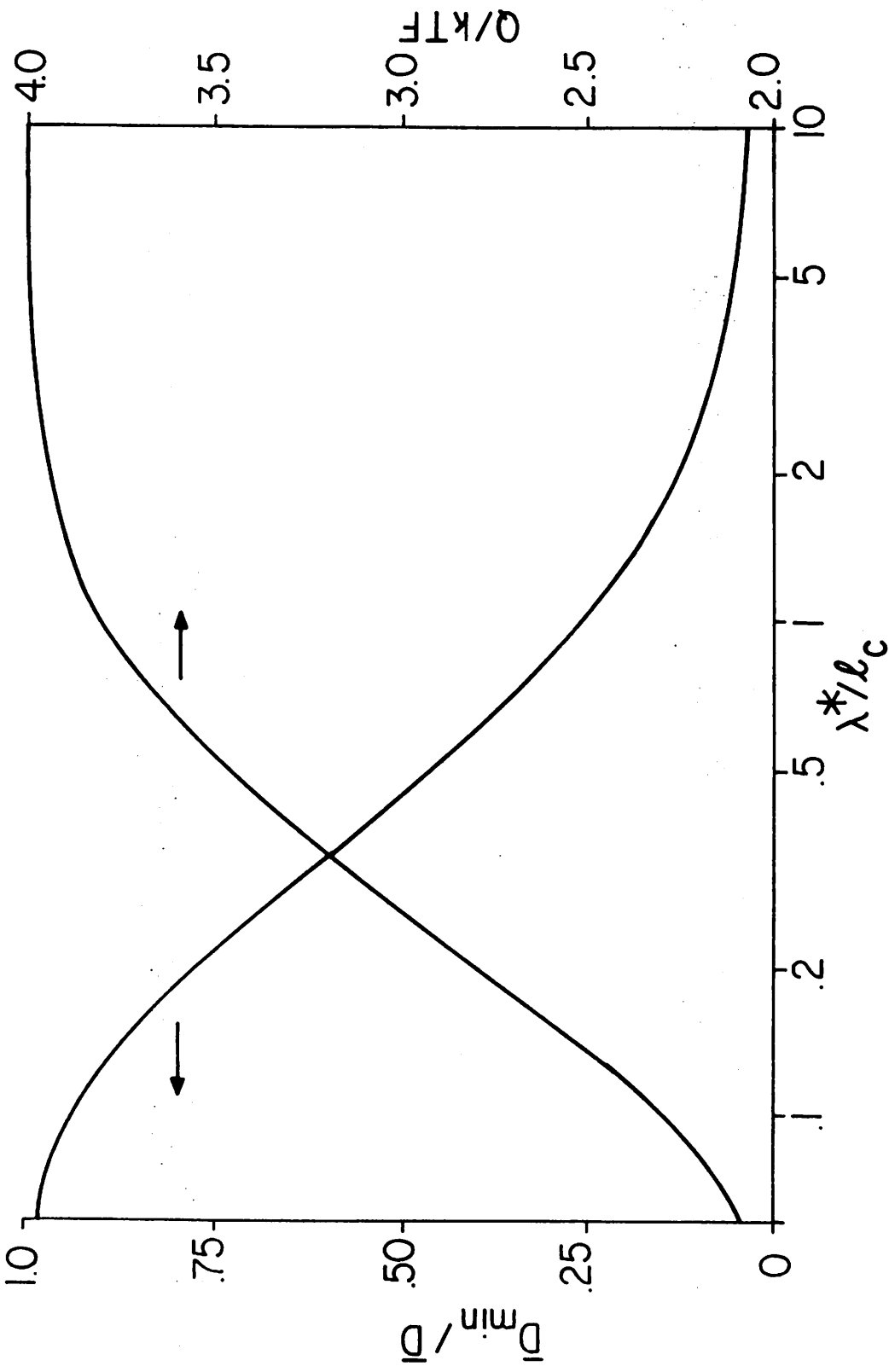


Fig. 2 Theoretical ratio of multiple-mirror diffusion coefficients \bar{D}_{\min}/\bar{D} , and ratio of energy loss flux Q to kT times the particle loss flux F , as a function of ratio of momentum transfer mfp λ^* to cell length l_c .

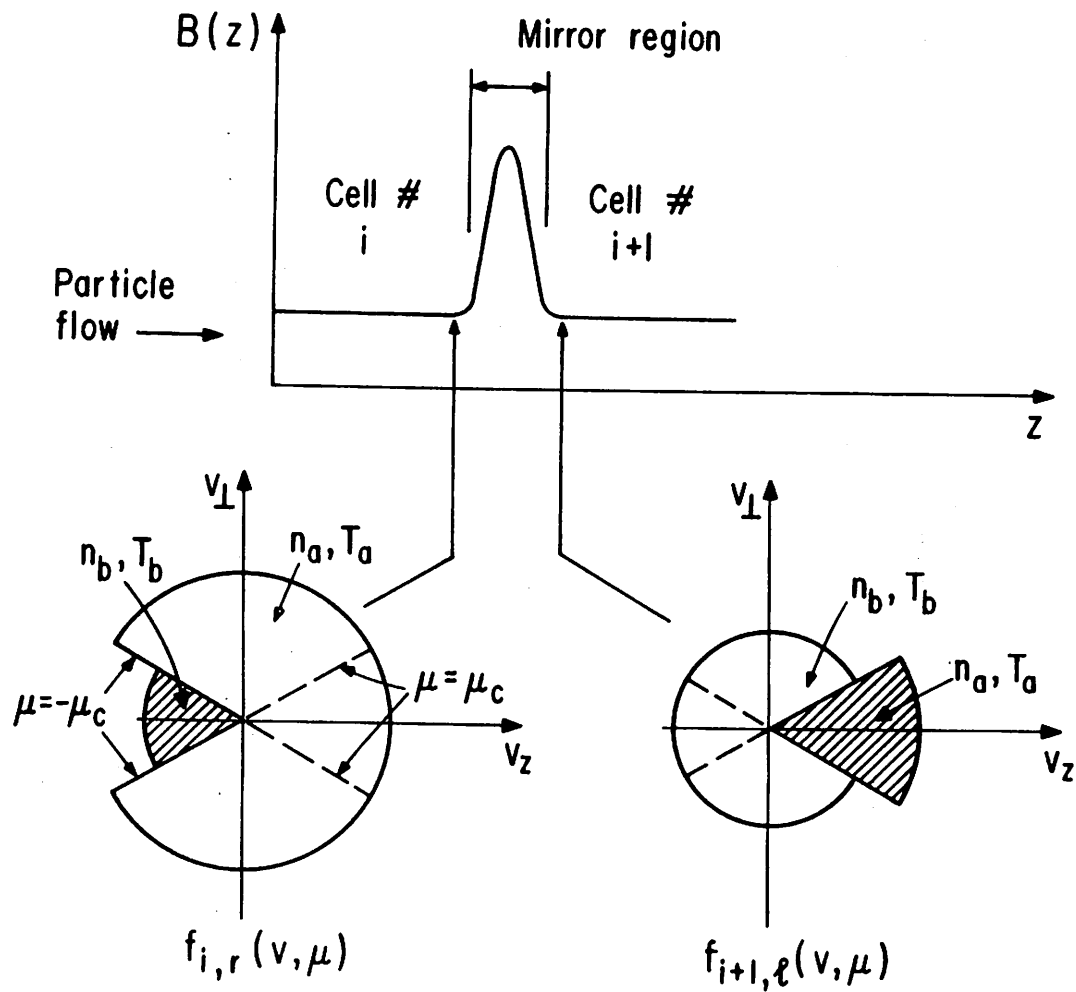


Fig. 3 Schematic representation of the distribution function on either side of a collisionless mirror

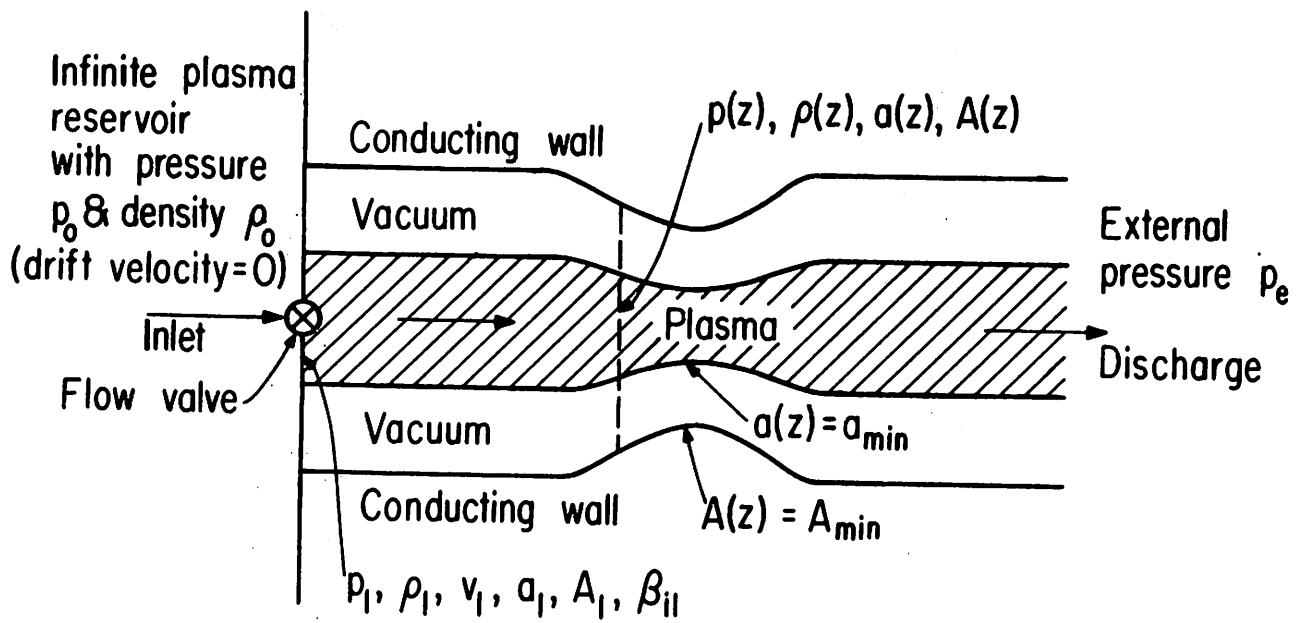


Fig. 4 A magnetic converging-diverging nozzle.

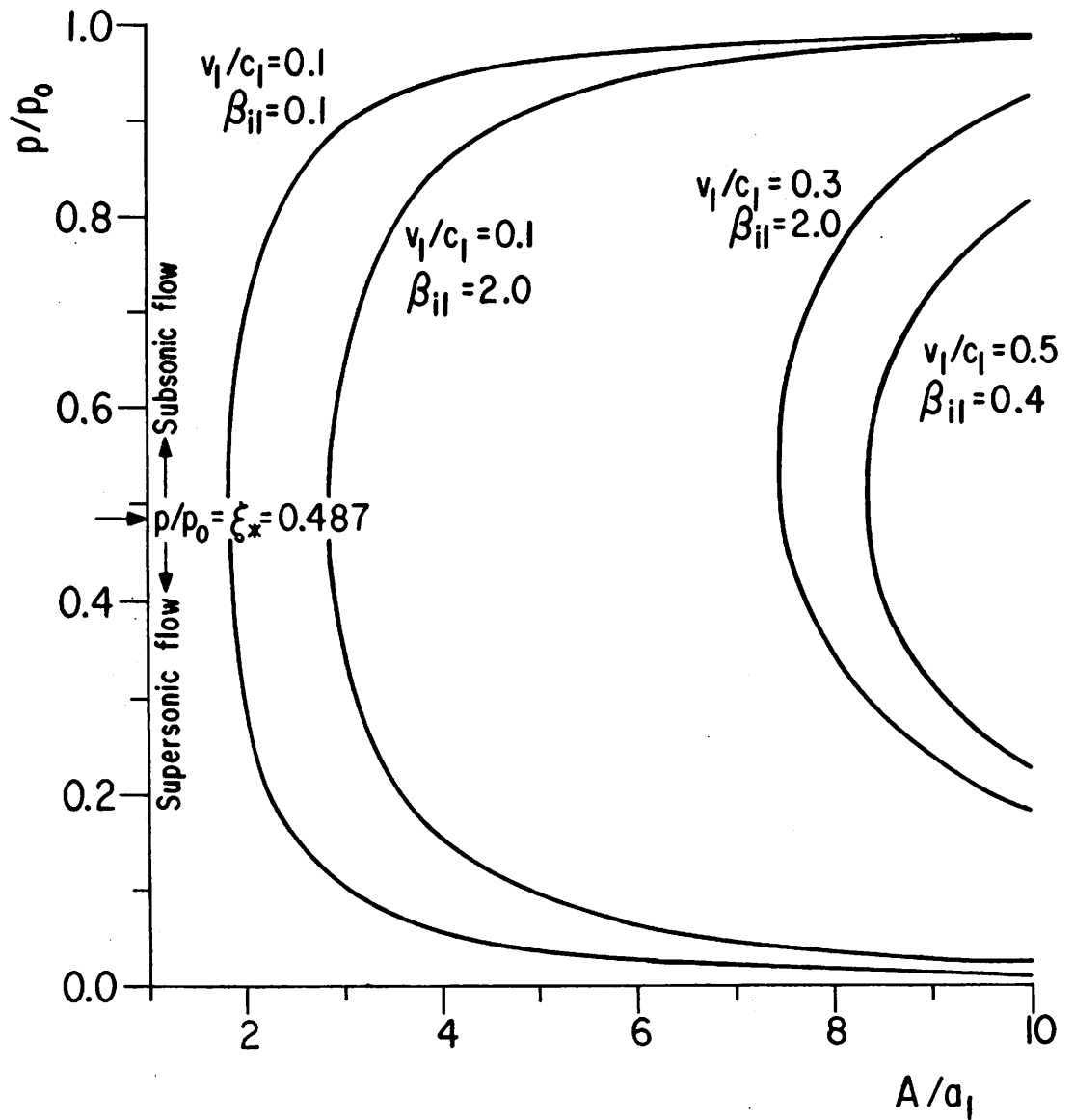


Fig. 5 Pressure variation in a converging-diverging magnetic nozzle

$$A_1/a_1 = 10, \gamma = 5/3$$

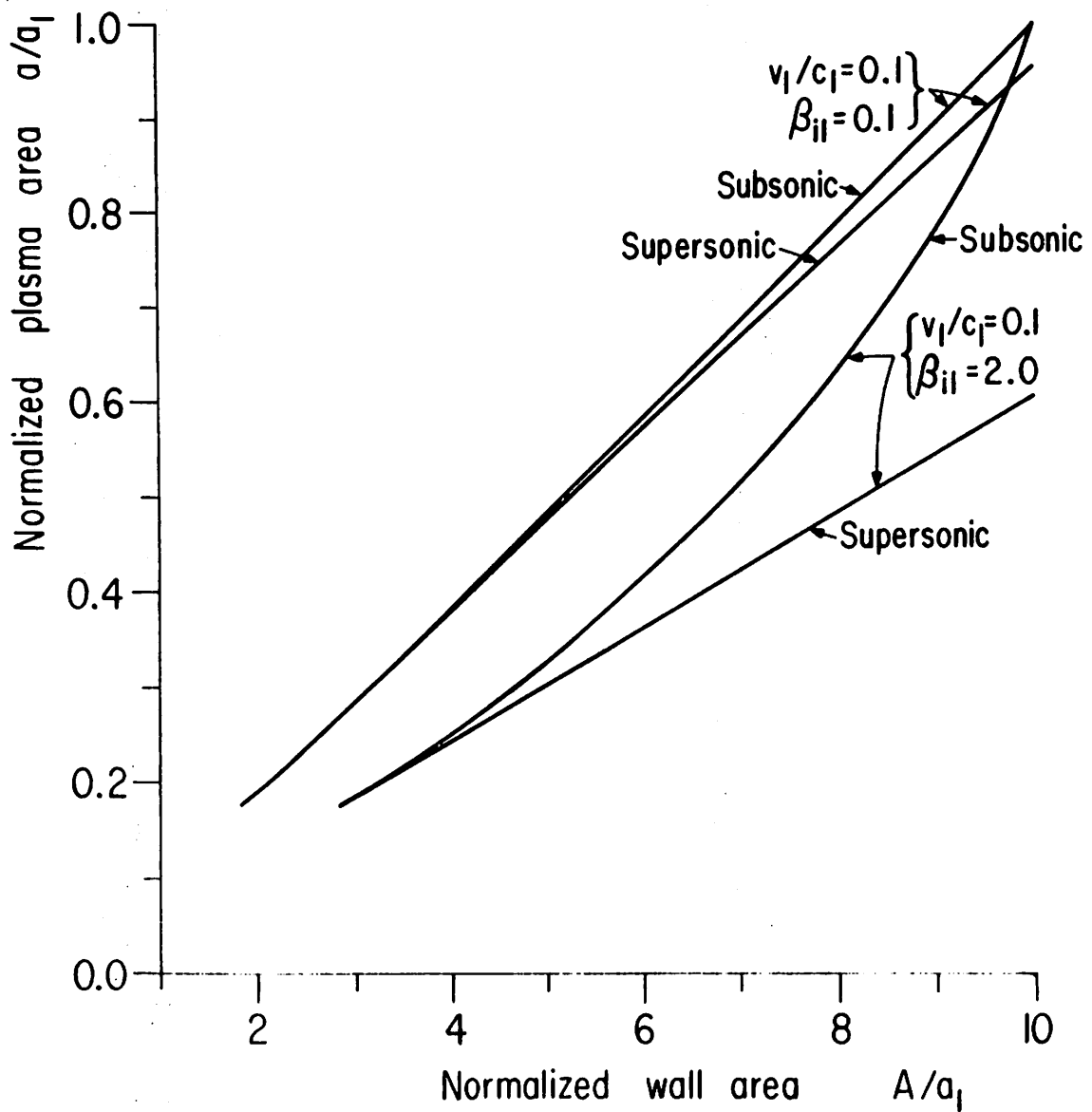


Fig. 6 Variation of plasma area with wall area for $A_1/a_1 = 10$, $\gamma = 5/3$.

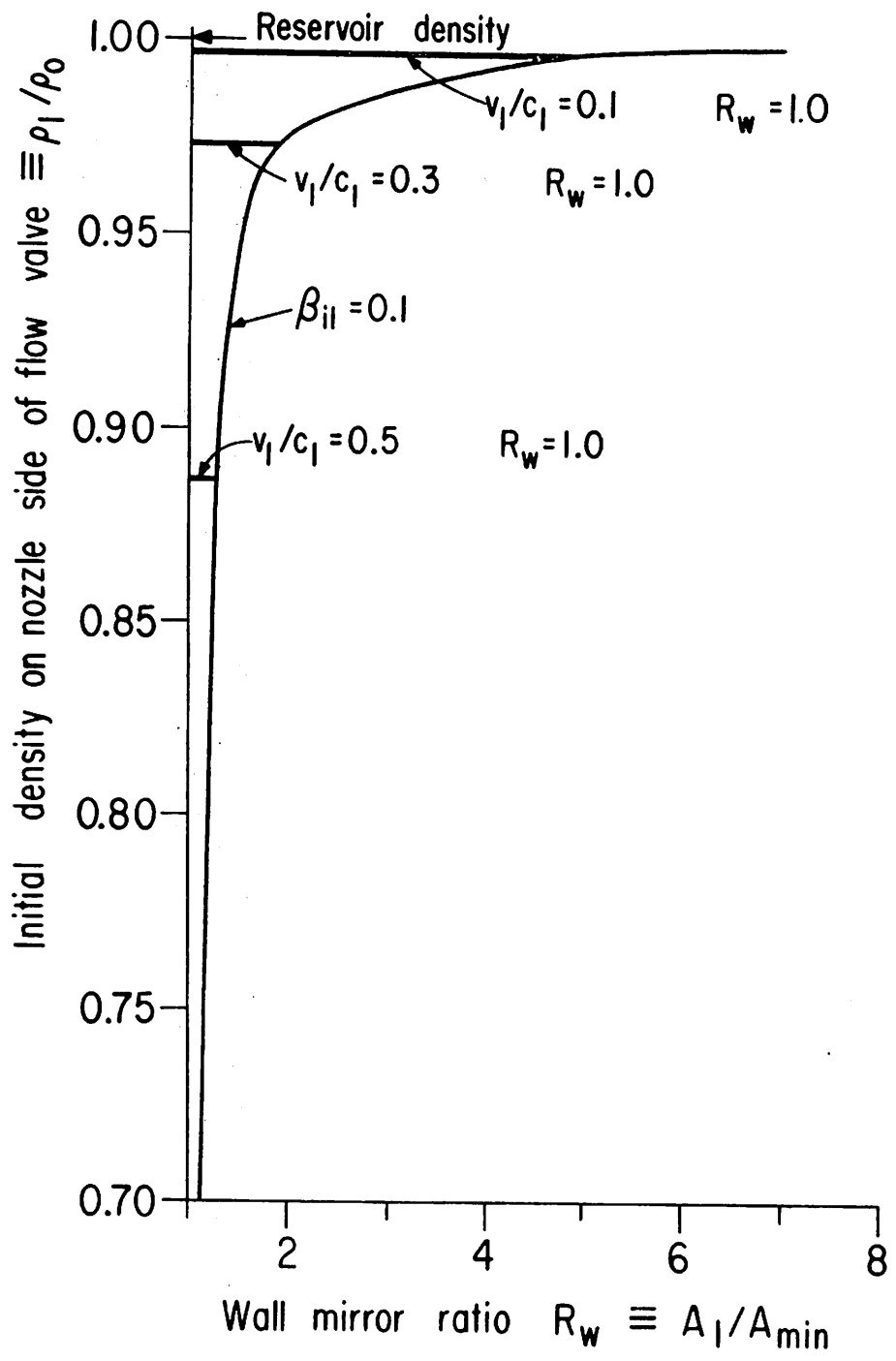


Fig. 7 Variation of initial density with wall mirror ratio (constant mass flow W).

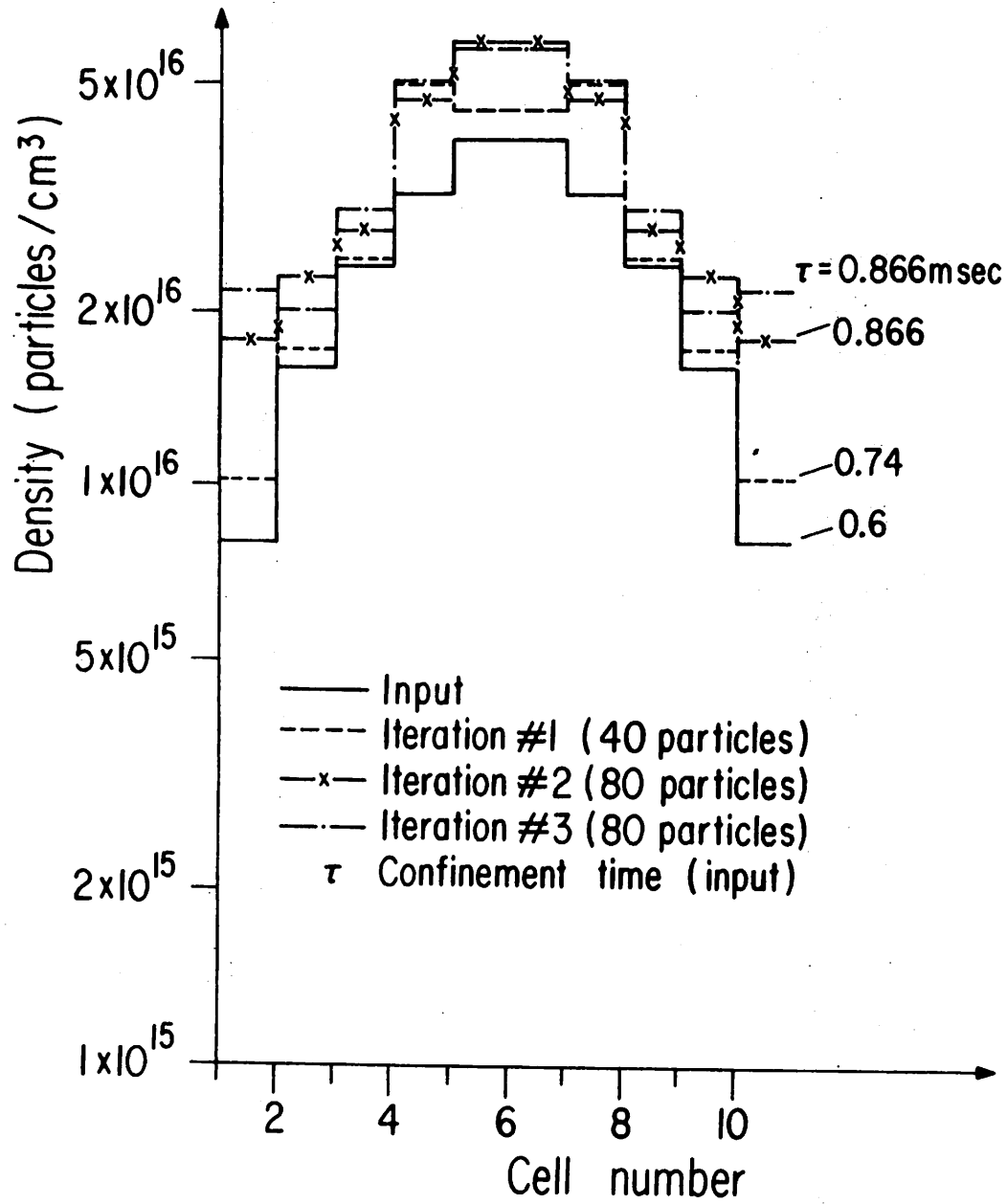


Fig. 8 Cell densities in a multiple mirror system; $S = 2.6 \cdot 10^{23}$ particles $\text{cm}^{-2} \text{sec}^{-1}$.

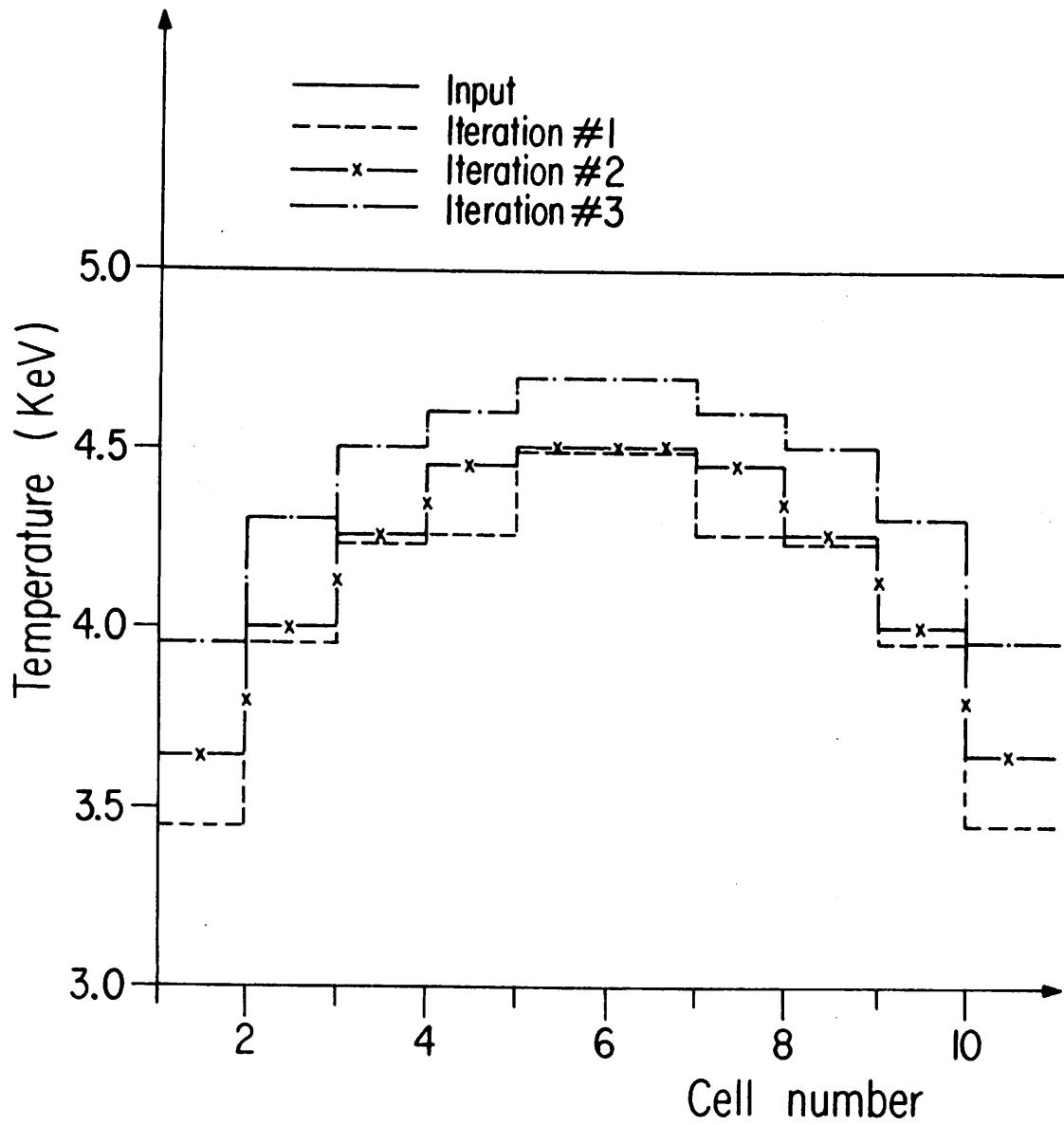


Fig. 9 Cell temperatures in a multiple mirror system; $S = 2.6 \cdot 10^{23}$ particles $\text{cm}^{-2} \text{sec}^{-1}$.

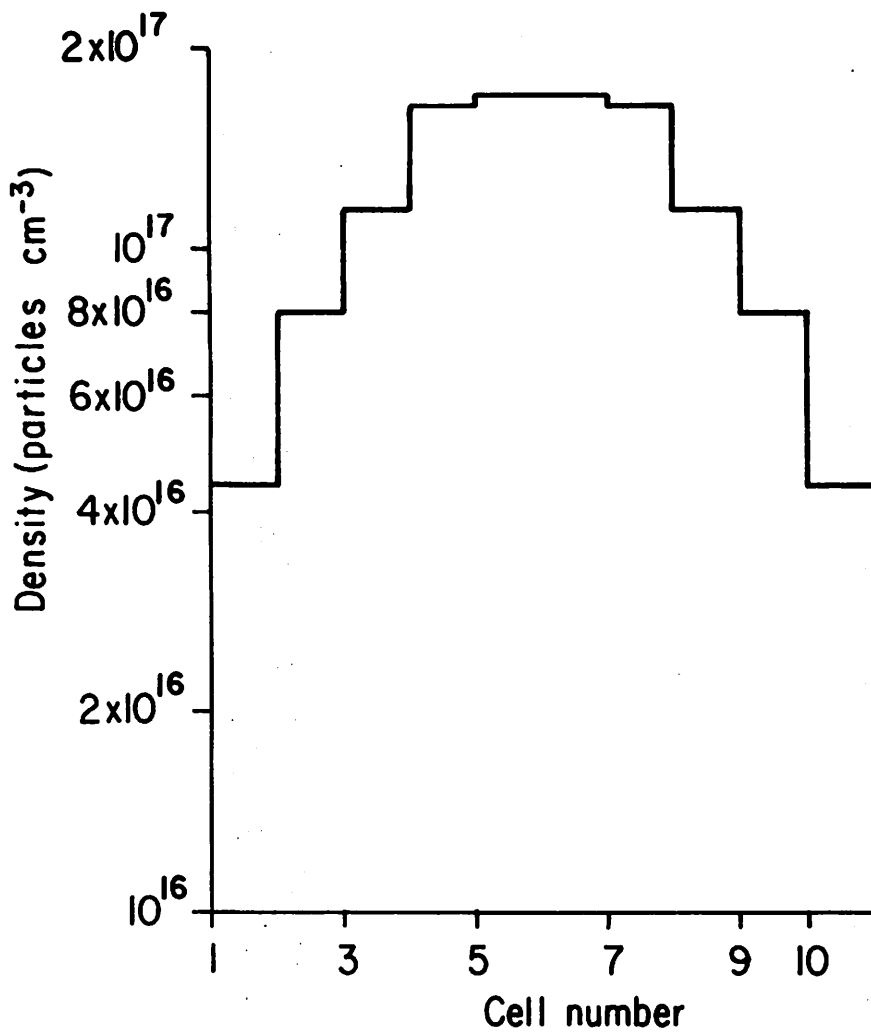


Fig. 10 Density profile for a 10 cell system with $M = 5$ and $S = 5 \times 10^{23}$ particles $\text{cm}^{-2} \text{sec}^{-1}$.

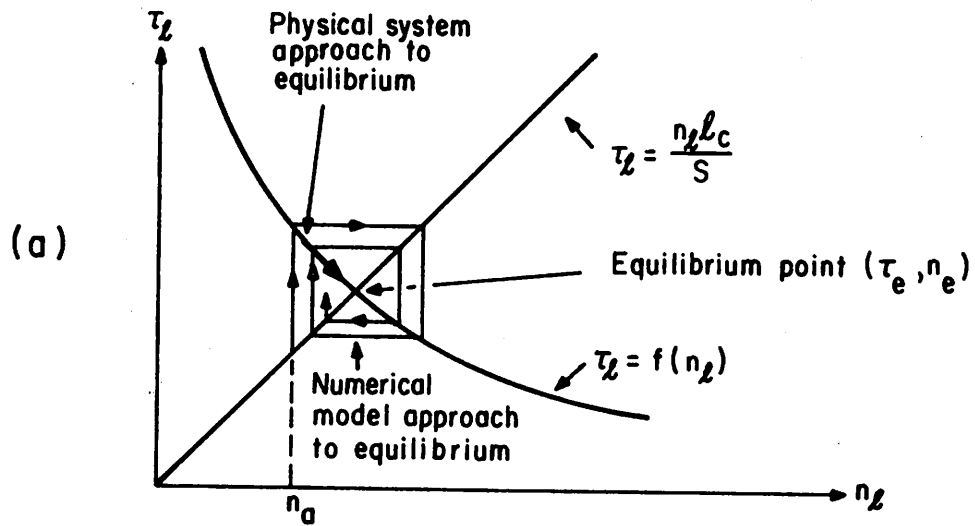


Fig. 11a Physical and numerical stability

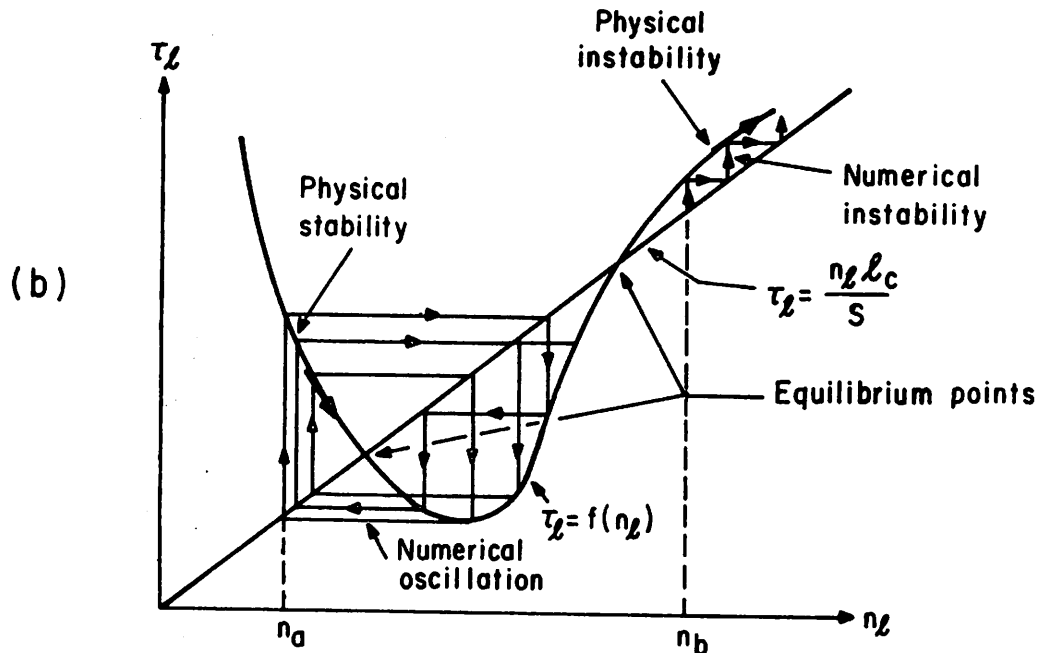


Fig. 11b Physical stability with numerical oscillation and physical and numerical instability.